

Cluster embedding in an elastic polarizable environment: Density functional study of Pd atoms adsorbed at oxygen vacancies of MgO(001)

Vladimir A. Nasluzov,^{a)} Vladimir V. Rivanenkov, and Alexey B. Gordienko^{b)}

Institute of Chemistry and Chemical Technology, Russian Academy of Sciences, 660049 Krasnoyarsk, Russia

Konstantin M. Neyman, Uwe Birkenheuer,^{c)} and Notker Rösch^{a)}

Institut für Physikalische und Theoretische Chemie, Technische Universität München, 85747 Garching, Germany

(Received 9 May 2001; accepted 8 August 2001)

Adsorption complexes of palladium atoms on F_s , F_s^+ , F_s^{2+} , and O^{2-} centers of MgO(001) surface have been investigated with a gradient-corrected (Becke–Perdew) density functional method applied to embedded cluster models. This study presents the first application of a self-consistent hybrid quantum mechanical/molecular mechanical embedding approach where the defect-induced distortions are treated variationally and the environment is allowed to react on perturbations of a reference configuration describing the regular surface. The cluster models are embedded in an elastic polarizable environment which is described at the atomistic level using a shell model treatment of ionic polarizabilities. The frontier region that separates the quantum mechanical cluster and the classical environment is represented by pseudopotential centers without basis functions. Accounting in this way for the relaxation of the electronic structure of the adsorption complex results in energy corrections of 1.9 and 5.3 eV for electron affinities of the charged defects F_s^+ and F_s^{2+} , respectively, as compared to models with a bulk-terminated geometry. The relaxation increases the stability of the adsorption complex Pd/ F_s by 0.4 eV and decreases the stability of the complex Pd/ F_s^{2+} by 1.0 eV, but it only weakly affects the binding energy of Pd/ F_s^+ . The calculations provide no indication that the metal species is oxidized, not even for the most electron deficient complex Pd/ F_s^{2+} . The binding energy of the complex Pd/ O^{2-} is calculated at -1.4 eV, that of the complex Pd/ F_s^{2+} at -1.3 eV. The complexes Pd/ F_s and Pd/ F_s^+ exhibit notably higher binding energies, -2.5 and -4.0 eV, respectively; in these complexes, a covalent polar adsorption bond is formed, accompanied by donation of electronic density to the Pd 5s orbital. © 2001 American Institute of Physics. [DOI: 10.1063/1.1407001]

I. INTRODUCTION

Various kinds of cluster models are successfully used in quantum chemical studies of solid surfaces of metals, semiconductors and insulators as well as of adsorption complexes on them.¹ Yet, the accuracy of cluster model techniques in practical applications is limited by uncertainties in the boundary conditions imposed on the clusters or by details of the cluster embedding. The cluster approach is especially advantageous for systems where the boundary conditions can be defined in a natural and transparent way. Whereas cluster embedding is inherently difficult for metals,² solid substances more amenable to cluster embedding are those (i) with directional covalent and polar covalent bonds (e.g., silicates and aluminosilicates) as well as those (ii) with sufficiently strong ionic bonds (e.g., the metal oxides MgO and Al_2O_3). These two classes of materials require different techniques to represent the appropriate cluster boundary conditions. In the first case, one may saturate dangling bonds at

the cluster border by monovalent pseudoatoms.³ In the second class of materials, the long-range Coulomb interaction between a cluster and its environment can significantly affect the properties of the local site under investigation and, therefore, has to be represented adequately in the computational model.⁴ For both classes of systems, the cluster environment can be considered to a good approximation as a classical system with its structural and elastic characteristics represented by a force field as utilized in atomistic simulations (AS) of solids⁵ or molecular mechanical (MM) descriptions of complex molecular systems.⁶ One may consider the Coulomb field due to the cluster environment to be generated by an array of classical point charges (PC) or, more generally, of point multipoles. This reasoning constitutes the logical basis for treating the above-mentioned classes of materials within a combined “quantum mechanical-molecular mechanical” (QM/MM) approach.^{3,7–10}

The fundamentals of a consistent cluster embedding for ionic solids have been developed a decade ago.¹¹ Nevertheless, for modeling surface sites of highly ionic materials (sometimes addressed as defects) only the simplest way of cluster embedding in rigid arrays of PC’s and pseudopotential ions has so far been employed in first-principle studies^{12–15} with one very recent exception where a shell-

^{a)} Authors to whom correspondence should be addressed.

^{b)} Permanent address: Department of Physics, Kemerovo State University, 650043 Kemerovo, Russia.

^{c)} Present address: Max-Planck Institut für Physik Komplexer Systeme, 01187 Dresden, Germany.

model embedding procedure has been applied to surface defects of MgO.⁹ Because the major effect of the surrounding on the QM cluster models is already reproduced by simple embedding in arrays of point charges, efforts seem to have been delayed to build a logically complete scheme that allows a variational treatment of the entire system, cluster plus environment. Thus, the present state of cluster models for ionic solids cannot be considered as fully satisfactory, in particular in comparison with the competing supercell approach employing periodic boundary conditions.^{16,17} Furthermore, such a simple embedding approach seems to be insufficient for considering more complex adsorption systems, e.g., adsorption at charged defects and polar surfaces, where adsorbate–substrate charge transfer can be significant and coupled with a substantial structural relaxation. This situation provides strong motivation for developing, implementing, and applying a hybrid QM/MM(AS) approach for modeling ionic materials and adsorption complexes at their surfaces. In this approach, a QM cluster is embedded in an elastic polarizable environment (EPE).^{9,10} This description of the environment incorporates features of the shell model^{11,18,19} which is widely used for solid state problems.^{5,20}

The central purpose of a classical treatment in such a QM/MM scheme is to obtain a reliable structure of a periodic system, e.g., of a model slab of the surface under study. This information can also be provided by a “first principles” treatment of a supercell model with periodic boundary conditions. In practice, such calculations require a substantial computational effort for moderately complex systems, and for truly complex systems this effort can become prohibitive. The MM(AS) approach is able to furnish structural data for rather complex systems.⁵ For a geometry determined at the MM level, the electrostatic interaction of the environment with the cluster can be approximated using the Madelung field of ions or PC’s. Via this interaction, observables of the site under investigation depend on the structure of the surface as a whole.²¹

The effect of the cluster “defect” on the substrate lattice can be rather strong (especially for charged surface sites) and has to be taken into account. A quantum mechanical treatment is required to properly represent the relaxation in the immediate vicinity of the defect. On the other hand, this relaxation results in a polarization of the environment which can be well described classically. If the structural relaxation of a cluster model is studied, the cluster and its environment have to be considered as one system in equilibrium. The energy of the system has to be optimized with respect to the positions of the nuclei of the cluster *and* of the surrounding ions. The resulting polarization of the environment constitutes an integral part of the embedding potential. It includes ion displacements within the shell-model array that describes the electronic polarization.^{18,22}

Several schemes for a self-consistent cluster embedding of ionic solids have been implemented.^{11,19,23–25} Many of these investigations^{11,24} employ a “first principles” Hartree–Fock treatment of cluster models which is based on the computer code ICECAP.²³ When elaborating an embedding technique, one has to pay careful attention to the interface region

between the QM and the classical MM parts of a model.^{11,23,25} Two aspects of this problem are worth recalling.

First, the boundary anions of the QM cluster, that are located in the immediate vicinity of positive PC’s of the environment, experience a strong artificial distortion of their electron density.^{12,13,26,27} Therefore, a cluster embedded in a PC array can exhibit an electron charge deficit; subsequently, the electrostatic field created by such a model can be erroneous, even to the point that the effect of embedding may be outweighed by these artifacts. This artificial polarization can be avoided if cations in the boundary region are represented by effective core pseudopotentials.^{13,27–30} These pseudopotential centers restore the otherwise missing short-range Pauli repulsion between the QM cluster and the classical environment. These modified centers can also be thought to provide a localizing potential that was introduced into embedding theory for formal reasons.^{31–34}

Second, substitution of a part of the classical medium by the QM cluster also results in an artificial distortion of the environment at the cluster boundaries. Therefore, a modification of the properties of the environment in the border region is required to restore the balance of forces that existed for each ion before the QM region was introduced. This problem can be tackled without modifying pair-potential parameters by invoking a special approach for constructing the interface model, which is considered an essential ingredient of the “elastic polarizable environment” (EPE) to be introduced in the following. In this QM/MM approach, the environment is allowed to respond to deviations of the geometric and electronic structure of the QM cluster from the reference ones. In Sec. II, we will introduce this novel method of interface coupling, implemented here in the density functional (DF) code PARAGAUS.³⁵

In this work, EPE embedding will be applied to study the adsorption of single Pd atoms at regular O²⁻ sites as well as on the oxygen vacancy sites F_s, F_s⁺, and F_s²⁺ of the MgO(001) surface. This paper extends previous systematic cluster model studies on the deposition of metal species at oxide substrates.^{36–41} The adsorption of Pd atoms on the regular O²⁻ sites is an example with essentially no adsorbate–substrate charge transfer; therefore, only minor effects of the adsorption-induced lattice relaxation are expected. In the case of the charged defects F_s⁺ and F_s²⁺, the Coulomb field of the vacancy provides a driving force for distorting the structure of both the cluster and its environment. For charged oxygen vacancies of MgO(001), rather high electron affinities have been calculated (up to 11.2 eV for F_s²⁺) [Ref. 42] when no, or only limited, relaxation due to the formation of the vacancy was taken into account.^{38,42} From this finding one would expect that electron density of the metal interacting with such a charged vacancy will be donated to the substrate, thus changing the relaxation pattern of the environment compared to that of an isolated defect. On the other hand, the relaxation of an isolated defect affects the electron affinity and in this way also influences the properties of the substrate. Electrons trapped by an F_s vacancy may be available for charge transfer in the opposite direction, i.e., to the adsorbate. This may also induce a significant re-

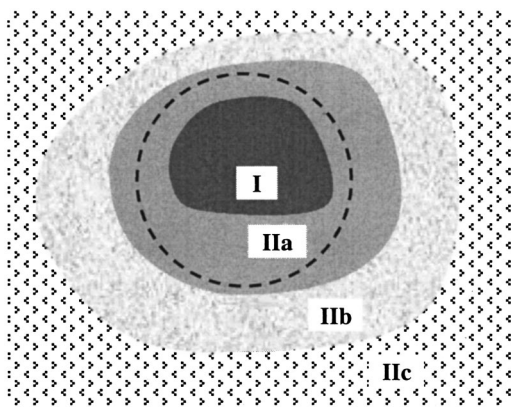


FIG. 1. Schematic representation of the space partitioning underlying a shell-model calculation on a bulk problem or an EPE embedded cluster model treatment of a surface site. I—region of the active site under study; II—regions of the environment. Region I consists (i) of discrete dipoles (shell-model ions) at the classical level, (ii) of the QM cluster (together with the pseudopotential frontier centers) at the quantum mechanical level. In Region IIa the positions of the polarizable shell-model ions are explicitly optimized. In Region IIb the polarization of the shell-model ions is taken into account in a harmonic approximation only. Region IIc is a dielectric medium (consisting of an infinite lattice of ions) polarizable by a monopole of the Region I. The sphere representing the auxiliary surface charge distribution to describe the Madelung field acting on the QM cluster is indicated by a dashed line.

laxation. The present hybrid QM/MM approach is expected to provide a well-founded procedure for calculating the properties of metal (M) adsorption complexes such as M/F_s , M/F_s^+ , and M/F_s^{2+} . These adsorption complexes are of interest as prototypes for supported catalysts representing the initial stage of metal deposition.^{43,44}

The paper is organized as follows. In Sec. II the EPE embedding strategy is outlined, followed by a discussion of computational details. In Sec. III the results of calculations on various sites at MgO(001) and on adsorption complexes with single Pd atoms are presented.

II. THE QM/EPE METHOD

A. Computational strategy

At the classical level, the energy and the structure of a point defect (labeled as Region I in Fig. 1) in a periodic system of ions are conveniently calculated with the help of a method introduced by Mott and Littleton^{18,20,45} where pair potentials describe the short-range mechanical interactions between the ions and the shell model²² determines the long-range Coulomb interactions including contributions due to the polarizability of discrete ions. In this approach, the environment of a defect (Region II; Fig. 1) is partitioned into three regions: (i) an inner Region IIa (where the positions of the ions are explicitly optimized), (ii) an intermediate Region IIb (where only an effective lattice polarization due to the effective charge of the defect is taken into account), and an outer Region IIc (see Fig. 1). In Regions IIa and IIb, the atomic structure of the polarized lattice (represented by an array of discrete dipoles) and the tensor character of its dielectric properties are taken into account. The effective polarization in Region IIb is described by means of harmonic (“Mott–Littleton”) displacements of the ions from their

equilibrium positions.¹⁸ Furthermore, one assumes that the energy of the defect is a quadratic function of the Mott–Littleton displacements in Region IIb.¹⁸ In this approximation the energy can be calculated by explicit summation over interactions among the ions of Regions I and IIa and between the ions of these two regions and those of Region IIb. The remaining, outer part of the outer region, Region IIc, is considered as a dielectric medium (consisting of an infinite lattice of ions), possibly polarized by a monopole located at the center of the defect; it contributes only to the energy of the defect, but not to the forces acting on ions of the inner regions.

The procedure of EPE embedding of a QM cluster is constructed in line with the concepts underlying the Mott–Littleton method. For the present hybrid QM/MM approach one partitions the whole system into the active region of the QM cluster *together* with the pseudopotential frontier centers (Region I) that allow a reduction of spurious effects due to the presence of a cluster boundary. Quantum mechanical and shell-model descriptions of the lattice polarizability for such highly ionic systems as MgO show acceptable agreement.⁴⁶ Nevertheless, one has to ensure that the coupling between the two regions (Region I—QM, Region II—MM) will not lead to significant structural distortions. The forces acting on atoms at the cluster border and on the neighboring EPE ions will not be balanced once the QM cluster is substituted for the inner region of the EPE system. These distortions can be minimized by using a special parameterization of the pair potentials for the interactions between the atomic nuclei of the QM cluster and the ions in the EPE regions as well as between the ions in Region II.²⁵ However, the main reason for such distortions is the difference in the charge density; therefore, the attempt to repair this deficiency by modifications of the force field alone is not well justified.

The EPE scheme suggested here, is designed such that a cluster which models a regular surface site leaves its crystal environment unperturbed. The difference in the electrostatic potential of clusters modeling the regular surface and the defect furnishes the main driving force for a lattice distortion close to the defect. The effect of the Coulomb potential of the EPE (defined by the lattice ion positions R_{lat}) on the QM cluster is computed explicitly. In addition to the regular atomic centers of the QM cluster at positions R_{cl} , the frontier pseudopotential centers located at positions R_{pp} are also assigned to the cluster. The role of these pseudopotentials (pp) is analogous to that of pseudoatoms saturating dangling bonds in the pseudobond embedding approach to covalent systems.⁴⁷

The following contributions to the total energy of the crystal, E_{tot} , are distinguished in the EPE cluster embedding procedure:

$$E_{tot} = E_{cl} + E_{int} + E_{lat}. \quad (1)$$

E_{cl} comprises the intracluster interactions, E_{int} describes the coupling of the QM cluster and the EPE, and, finally, E_{lat} designates the intralattice interactions. The following preparatory computational Steps 1 and 2 have to be performed before one can carry out the final QM/EPE Step 3.

Step 1—Pure MM(AS) treatment of the *regular* (unperturbed) surface.

The equilibrium geometry of the unperturbed surface is produced by minimizing the total energy E_{tot}^{MM} of an entire slab (repeated periodically) in the shell-model approach.¹⁸ That energy depends on the coordinates R of the ions and their effective dipole moments μ :

$$E_{\text{tot}}^{MM}(R, \mu) \xrightarrow{\text{minimization}} R^{reg}, \mu^{reg}. \quad (2)$$

In fact, each shell-model ion is represented by a pair of PC's of opposite signs (a core and a shell) connected by a "spring" with properly adjusted force constant to describe

the polarizability of the ion in an external electrostatic field;¹⁸ thus, the model does not employ point dipoles. Step 1 generates the EPE reference geometry (and the electrostatic potential) of the regular surface (hence the superscript *reg*), unperturbed by any surface defect or adsorbate.

It is crucial for the following to differentiate between three types of ions: those at the regular centers, R_{cl} , of the QM cluster, those ions at the pseudopotential centers, R_{pp} , and those at lattice positions of the environment (Regions II), R_{lat} . In Steps 2 and 3, the shell-model ions of Region I (Fig. 1) will be substituted by real QM ions or pseudopotential ions. Hence Eq. (2) is recast as

$$E_{\text{tot}}^{MM}(R_{cl}, R_{pp}, R_{lat}, \mu_{cl}, \mu_{pp}, \mu_{lat}) \xrightarrow{\text{minimization}} R_{cl}^{reg}, R_{pp}^{reg}, R_{lat}^{reg}, \mu_{cl}^{reg}, \mu_{pp}^{reg}, \mu_{lat}^{reg}, \rho_{cl}^{\text{tot}, MM}(R_{cl}^{reg}, R_{pp}^{reg}, \mu_{cl}^{reg}, \mu_{pp}^{reg}). \quad (3)$$

The optimized coordinates and dipole moments of the shell-model ions in Region I as well as the electrostatic potential of the resulting charge distribution, $\rho_{cl}^{\text{tot}, MM}(R_{cl}^{reg}, R_{pp}^{reg}, \mu_{cl}^{reg}, \mu_{pp}^{reg})$ will be used as a reference in Step 3. The configuration of the shell-model ions in Regions II will be used in Step 2.

Step 2—QM *reference* calculation of the cluster (Region I) *embedded* in the *regular* (unperturbed) environment represented by the frozen lattice configuration $R_{lat} = R_{lat}^{reg}, \mu_{lat} = \mu_{lat}^{reg}$ (Region II).

Let us first consider the energy expression

$$E_{\text{clean surface}}^{QM, reg, emb}(\rho_{cl}, R_{cl}, R_{pp}) = E_{cl} + E_{int}^{bare} \\ E_{cl} = E^{QM}(\rho_{cl}, R_{cl}) + tr(\rho_{cl} V_{pp}(R_{pp})) + V_{nn}^{mod}(R_{cl}, R_{pp}) \\ E_{int}^{bare} = [\rho_{cl}^{\text{tot}, QM}(\rho_{cl}, R_{cl}, R_{pp}) \| \rho_{lat}(R_{lat}^{reg}, \mu_{lat}^{reg})] \\ + V_{short}(R_{cl}, R_{pp}, R_{lat}^{reg}), \quad (4)$$

where ρ_{cl}^{tot} and ρ_{cl} are the total charge distribution (i.e., electron density plus atomic nuclei) and the electron only contribution of Region I; ρ_{lat} is the total charge density of Region II, comprised of the core and shell charges of all those shell-model ions. By $tr(\rho V)$ we denote the interaction energy of an electronic charge distribution ρ in a potential V ; $[\rho_1 \| \rho_2]$ designates the Coulomb interaction energy between the charge distributions ρ_1 and ρ_2 . Besides the genuine quantum mechanical cluster contribution E^{QM} , the cluster energy E_{cl} comprises the interaction of the cluster electronic charge density ρ_{cl} with the field V_{pp} of the pseudopotential centers and a modified nuclear repulsion term V_{nn}^{mod} between the atoms of the cluster and the pseudopotential centers at R_{pp} . This modification is necessary to counter possible deficiencies of the pseudopotential description when reproducing the geometry of the QM cluster (see the following). The interaction energy E_{int}^{bare} contains the Coulomb interaction between

the (total) charge distributions of both regions as well as a short-range term V_{short} which represents an adapted shell-model interaction (for details see the following).

That latter potential energy originates from the genuine short-range interaction contributions to the inter-region coupling energy E_{int} of the shell model. Optimizing the energy expression given in Eq. (4) with respect to the electronic charge density ρ_{cl} and the positions of the cluster ions R_{cl} and R_{pp} (by a series of QM calculations) provides the *reference* configuration (hence the notation *ref*) of the quantum mechanical cluster model of the unperturbed clean surface:

$$E_{\text{clean surface}}^{QM, reg, emb}(\rho_{cl}, R_{cl}, R_{pp}) \xrightarrow{\text{minimization}} \rho_{cl}^{ref}, R_{cl}^{ref}, R_{pp}^{ref}, \rho_{cl}^{\text{tot}, QM}(\rho_{cl}^{ref}, R_{cl}^{ref}, R_{pp}^{ref}). \quad (5)$$

Note that the total charge distribution of the reference configuration $\rho_{cl}^{\text{tot}, QM}(\rho_{cl}^{ref}, R_{cl}^{ref}, R_{pp}^{ref})$ obtained here is quite different from the total charge distribution $\rho_{cl}^{\text{tot}, MM}(R_{cl}^{reg}, R_{pp}^{reg}, \mu_{cl}^{reg}, \mu_{pp}^{reg})$ associated with Region I by the pure MM(AS) treatment of the clean surface in Step 1—and so are the electrostatic potentials experienced by the surrounding environment.

Step 3—The final QM/EPE calculation. Minimization of the total energy expression

$$E_{\text{tot}}^{bare} = E_{cl} + E_{int}^{bare} + E_{lat} \\ E_{lat} = E_{intra-lat}^{MM}(R_{lat}, \mu_{lat}) \quad (6)$$

would result in a *relaxation* of Region II—even *without any defect* because $\rho_{cl}^{\text{tot}, MM}(R_{cl}^{reg}, R_{pp}^{reg}, \mu_{cl}^{reg}, \mu_{pp}^{reg})$ from Eq. (3) and $\rho_{cl}^{\text{tot}, QM}(\rho_{cl}^{ref}, R_{cl}^{ref}, R_{pp}^{ref})$ from Eq. (5) differ. This energy expression is thus not suitable. To avoid this artifact we modify the interaction expression E_{int}^{bare} by defining an effective (total) charge density $\rho_{cl}^{\text{tot}, eff}(\rho_{cl}, R_{cl}, R_{pp})$ to be used in place of $\rho_{cl}^{\text{tot}, QM}$ in Eq. (6) such that, for a defect-free system in its

reference configuration, $\rho_{cl}^{\text{tot,eff}}$ coincides with the charge density $\rho_{cl}^{\text{tot,MM}}(R_{cl}^{\text{reg}}, R_{pp}^{\text{reg}}, \mu_{cl}^{\text{reg}}, \mu_{pp}^{\text{reg}})$ of the substrate in its regular structure:

$$\begin{aligned} \rho_{cl}^{\text{tot,eff}}(\rho_{cl}, R_{cl}, R_{pp}) &= \rho_{cl}^{\text{tot,QM}}(\rho_{cl}, R_{cl}, R_{pp}) \\ &\quad - \rho_{cl}^{\text{tot,QM}}(\rho_{cl}^{\text{ref}}, R_{cl}^{\text{ref}}, R_{pp}^{\text{ref}}) \\ &\quad + \rho_{cl}^{\text{tot,MM}}(R_{cl}^{\text{reg}}, R_{pp}^{\text{reg}}, \mu_{cl}^{\text{reg}}, \mu_{pp}^{\text{reg}}). \end{aligned} \quad (7)$$

Analytic representations of $\rho_{cl}^{\text{tot,MM}}(R_{cl}^{\text{reg}}, R_{pp}^{\text{reg}}, \mu_{cl}^{\text{reg}}, \mu_{pp}^{\text{reg}})$ and $\rho_{cl}^{\text{tot,QM}}(\rho_{cl}^{\text{ref}}, R_{cl}^{\text{ref}}, R_{pp}^{\text{ref}})$ generated in Steps 1 and 2, respectively, are used to construct $\rho_{cl}^{\text{tot,eff}}$ in the final QM/EPE calculations. Similarly, we define an effective short-range potential:

$$\begin{aligned} V_{\text{short}}^{\text{eff}}(R_{cl}, R_{pp}, R_{lat}) &= V_{\text{short}}(R_{cl}, R_{pp}, R_{lat}) \\ &\quad - V_{\text{short}}(R_{cl}^{\text{ref}}, R_{pp}^{\text{ref}}, R_{lat}) \\ &\quad + V_{\text{short}}(R_{cl}^{\text{reg}}, R_{pp}^{\text{reg}}, R_{lat}). \end{aligned} \quad (8)$$

Again, in the absence of any surface defects, $V_{\text{short}}^{\text{eff}}(R_{cl}, R_{pp}, R_{lat})$ coincides with $V_{\text{short}}(R_{cl}^{\text{reg}}, R_{pp}^{\text{reg}}, R_{lat})$. We now define a modified coupling energy expression $E_{\text{int}}^{\text{eff}}$ in analogy to $E_{\text{int}}^{\text{bare}}$:

$$\begin{aligned} E_{\text{int}}^{\text{eff}} &= [\rho_{cl}^{\text{tot,eff}}(\rho_{cl}, R_{cl}, R_{pp}) \| \rho_{lat}(R_{lat}, \mu_{lat})] \\ &\quad + V_{\text{short}}^{\text{eff}}(R_{cl}, R_{pp}, R_{lat}), \end{aligned} \quad (9)$$

where the first term represents the Coulomb interaction of Regions I and II. Note that this modification of the total energy has no direct consequences on the QM treatment because the electronic charge density ρ_{cl} only enters the effective charge density $\rho_{cl}^{\text{tot,eff}}$ via the bare QM cluster charge density $\rho_{cl}^{\text{tot,QM}}$. Finally, the EPE total energy expression of the whole system to be minimized reads [see Eq. (6)]:

$$\begin{aligned} E_{\text{tot}}^{\text{EPE}} &= E_{cl} + E_{\text{int}}^{\text{eff}} + E_{lat} \\ E_{\text{tot}}^{\text{EPE}}(\rho_{cl}, R_{cl}, R_{pp}, R_{lat}, \mu_{lat}) \end{aligned} \quad (10)$$

$$\begin{aligned} \text{minimization} \\ \Rightarrow R_{cl}^{\text{EPE}}, R_{pp}^{\text{EPE}}, R_{lat}^{\text{EPE}}, \rho_{cl}^{\text{EPE}}, \mu_{lat}^{\text{EPE}}. \end{aligned}$$

The terms in the energy expression, Eq. (10), can be regrouped to yield:

$$\begin{aligned} E_{\text{tot}}^{\text{EPE}} &= E_{cl} + E_{\text{int}}^{\text{bare}} + E_{lat}^{\text{eff}} \\ E_{\text{lat}}^{\text{eff}} &= E_{lat} + E_{\text{int}}^{\text{corr}}. \end{aligned} \quad (11)$$

Here, $E_{\text{int}}^{\text{corr}}$ contains the correction terms to $E_{\text{int}}^{\text{eff}}$ which do not depend on the actual electronic and geometric structure of the cluster ($\rho_{cl}, R_{cl}, R_{pp}$) and thus can formally be reassigned to the intralattice energy expression.

The QM/EPE approach with consistent embedding allows to build a multifunctional model of an isolated site by means of unconstrained geometry optimization where nevertheless the polarization of the cluster surrounding is fully taken into account. With this strategy, also complex systems, e.g., those formed by reconstruction of polar surfaces,⁴⁸ can be modeled. A fundamental goal of the EPE approach is that the equilibrium geometry of a cluster simulating a regular

crystal is close enough to the geometry of the corresponding fragment of an infinite lattice, e.g., as described by a quantum mechanical calculation of the unperturbed system. Therefore, a necessary condition for the success of the EPE procedure is that the structure of the unperturbed substrate as determined by the MM(AS) treatment (i.e., the *regular* structure; Step 1) is close to the reference, provided by either experiment or a full high-level quantum mechanical treatment.

The fact that EPE represents a consistent embedding methodology permits one to tune parameters of the pair-potential functions such that observables fit the values calculated with a “first principles” approach. Thus, the structural as well as electrostatic and elastic characteristics of an EPE surface cluster model can be improved step by step.⁴⁹ Recent experiments on selected oxide materials indicate significant differences between the properties of surface and bulk atoms;⁵⁰ this finding may justify specific modifications of MM(AS) parameters originally developed for describing bulk systems.

B. Computational details

The QM calculations were carried out with the linear combination of Gaussian-type orbitals fitting-functions density-functional method (LCGTO-FF-DF)⁵¹ implemented in the parallel computer code PARAGAUSS^{35,52} using the generalized gradient approximation of the exchange-correlation functional as suggested by Becke and Perdew (BP).^{53,54}

Relativistic effects for the species containing a Pd atom were accounted for by either applying the Douglas–Kroll scalar relativistic approach to the Dirac–Kohn–Sham problem^{55,56} or via relativistic pseudopotentials.^{57,58} In some cases, “Stuttgart” pseudopotentials were used for the O²⁻ ions⁵⁹ and Mg²⁺ centers.⁶⁰ The latter were also used for the (Mg^{pp*})²⁺ centers, but without basis functions. Here and below we use the notation *pp** to denote bare pseudopotential centers; from a formal point of view, they do not affect the electronic structure (or the stoichiometry) of the cluster model since they neither bear any basis functions nor generate any new atomic states which would be able to participate in the formation of cluster molecular orbitals and thus withdraw electronic density from the genuine cluster. In the all-electron calculations, the following Gaussian-type orbital basis sets were employed: Mg(15s10p1d)→[6s5p1d], O(13s8p1d)→[6s5p1d], Pd(18s13p9d→7s6p4d).^{36,38} In the LCGTO-FF-DF method the classical Coulomb contribution to the electron-electron interaction is evaluated with a representation of the electronic charge density by an auxiliary Gaussian basis set which was constructed in a standard fashion by scaling orbital exponents of the orbital basis set; on each atomic center, this set was augmented by either 5 *p*-type (Mg, O) or 5 *p*- and 5 *d*-type (Pd) “polarization” exponents, each forming a geometric series with a multiplicative spacing of 2.5, starting at 0.1 and 0.2 au, respectively.⁵¹ The oxygen basis set was also used to describe the electrons trapped by the oxygen vacancy. The adsorbate–substrate binding energies were corrected for the basis set superposition errors (BSSE) by applying the counterpoise method⁶¹ in single-point fashion at the equilibrium geometry of the sur-

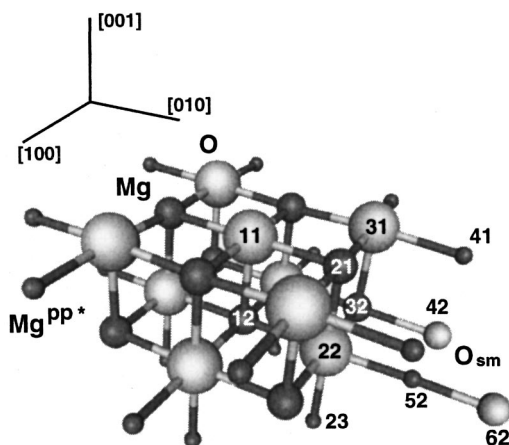


FIG. 2. Sketch of the standard cluster $[\text{Mg}_9\text{O}_9]\text{Mg}_{16}^{pp*}$ modeling an O^{2-} site of the $\text{MgO}(001)$ surface. Numbering ($i_m j_n$) of symmetry inequivalent ionic positions i_m of the cluster in the top ($j_n=1$) or second ($j_n=2$) layer of the cluster; see text for details. The shell-model centers O_{sm} (42) and (62) are given for easy reference, but are not part of the standard cluster; no further shell-model centers are shown for clarity. For a definition of the bare pseudopotential centers Mg^{pp*} see Computational Details.

face complexes. In scalar relativistic calculations, contributions due to bare and regular pseudopotential atoms (if used) were added to the Kohn–Sham Hamiltonian after the relativistic transformations.⁵⁶

A six-layer slab was chosen for modeling the regular O^{2-} site and the oxygen vacancies on the (001) surface of MgO . The five-coordinated O^{2-} site was represented by the standard cluster $[\text{O}_9\text{Mg}_9]\text{Mg}_{16}^{pp*}$ of C_{4v} point group symmetry. The top-most (surface) layer of the cluster centered on the oxygen anion consists of the moiety $\text{O}-\text{Mg}_4-\text{O}_4-\text{Mg}_8^{pp*}$, where the three coordination spheres of the central O atom are listed separated by dashes. The second and third layers of the standard cluster are $\text{Mg}-\text{O}_4-\text{Mg}_4-\text{Mg}_4^{pp*}$ and Mg_4^{pp*} , respectively (see Fig. 2). Other model clusters, mostly subsets of the standard cluster, were used to study the effects of cluster size and the representation of cations in the boundary region of the QM cluster.

For treating the EPE around the cluster model, a variant of the shell-model MM(AS) scheme¹⁸ was implemented as a module of PARAGAUSS.^{35,52} The shell-model parameters of the MM(AS) energy expression⁶² reproduce the experimental geometry and the elastic constants of MgO crystals. The charges of cations and anions are set to their formal values of ± 2 e. In the present scheme, it is possible to render these parameters internally consistent with the charge separation of the QM calculations.^{25,63} Such QM-consistent charge parameters would minimize the artificial distortion in the frontier region between the cluster and its environment. However, in the EPE approach this specific strategy⁴⁹ does not have to be invoked since by construction (see Sec. II A) such distortions do not play a major role.

For ionic substrates, an accurate representation of the Madelung potential of the extended system is crucial. In all EPE calculations, in particular during the EPE iterations of Step 3, the Madelung field of the complete system is always

determined in an accurate fashion using standard algorithms with summations in direct and reciprocal space.^{4,64} In Step 1 of the QM/EPE procedure, a rigid ion approximation is applied when the equilibrium structure of slab models of the $\text{MgO}(100)$ surface are calculated; thus, the ions are not allowed to become polarized under the influence of surface effects. Then Regions I and IIa are relaxed to equilibrium allowing a polarization of the anions according to the shell model. After Step 1, the Madelung potential of this reference system acting on the QM cluster is represented with the help of an auxiliary surface charge density on a sphere that encompassed Region I.⁶⁵ To achieve high accuracy, this auxiliary sphere should be used to represent an extended system from which a neutral part located in symmetric fashion around the QM cluster has been removed. The contribution of that missing section to the Madelung field as well as all changes of the field due to modifications of the environment as described by the EPE procedure are explicitly taken into account via the effect of a PC array surrounding the QM model cluster. Recall that, in Region IIa, the positions of “cores” and “shells” representing the ions and their dipole moments in the shell-model treatment are relocated to their equilibrium positions during Step 3 of the EPE procedure. In Region I, the locations of all centers and the electronic charge distribution change with each QM geometry cycle. As overall consequence of this approach, all changes of the Madelung field due to changes in Regions IIa and IIb (relevant to the QM and EPE calculations) as well as in Region I (relevant to the EPE calculations) are accounted for.

For all cluster models used, the sphere representing the auxiliary surface charge distribution has a radius 7 Å and is centered on the regular O^{2-} surface site. The neutral section of the regular substrate removed from the regular slab contains 34 centers of Region I and 516 ions of Regions IIa and IIb. The surface charge density is represented by a grid of 110 point charges;⁶⁶ the values of these PC’s are determined according to a matrix inversion procedure⁶⁵ based on the exactly calculated Madelung potential of the regular slab system.

Substrate ions are assigned to the inner EPE Region IIa if they are located less than $R_{IIa}=5$ Å from any center of Region I. For embedding the standard cluster $[\text{O}_9\text{Mg}_9]\text{Mg}_{16}^{pp*}$, Region IIa contains 171 ions. Region IIb is constructed similarly with a defining distance of at most $R_{IIb}=18$ Å from any of the centers in Region I, but excluding any centers already assigned to Regions I and IIa; for the standard cluster, Region IIa contains 1902 ions. The ion displacements in Region IIb are determined according to the Mott–Littleton prescription⁴⁵ using the dielectric constant of bulk MgO , $\epsilon=9.86$.⁶⁷

We also need to define V_{nn}^{mod} in Eq. (4) to adapt the short-range interaction between bare pseudopotential centers and their nearest-neighbor anion centers of Region I for a full geometry optimization. The correction of this term compensates for the reduced accuracy of the quantum mechanical description provided by these bare pseudopotential centers and minimizes distortions at the cluster frontier for the model of a regular site (Fig. 2). To do so, the short-range interactions of the centers $(\text{Mg}^{pp*})^{2+}$ with their nearest-neighbor

TABLE I. Pair potential functions of Buckingham-type with parameters A, B, and C for correcting the interaction of bare pseudopotentials (Mg^{pp*})²⁺ with normal oxygen centers of the QM cluster (P1), V_{nn}^{mod} [see Eq. (3)], and the short-range interactions (P2), V_{short} , of the cluster-EPE coupling (see Fig. 2).

	P1 ^a	P2 ^b	P2 ^b
Interaction	$Mg^{pp*}-O$	$Mg-O_{sm}$	$Mg^{pp*}-O_{sm}$
Reference atom pair	(11)–(21)	(12)–(22)	(12)–(22)
Target atom pair	(31)–(41)	(32)–(42)	(52)–(62)
Center displaced	O	Mg	Mg^{pp*}
Direction	$[\bar{1}10]$	[100]	[100]
A, au	2.265	55.16	55.31
B, au	1.022	0.5724	0.5833
C, au	110.3	51.61	51.67

^aP1: parameters of V_{nn}^{mod} optimized.

^bP2: parameters of V_{short} optimized.

anions were parameterized using analytical pair potentials of the Buckingham-type, $f(r) = A \exp(-Br) + Cr^{-6}$. The parameters were determined by minimizing the difference (in a least-squares sense) between reference and target potential energy curves of displacements in $[\bar{1}10]$ direction of the O^{2-} anion at regular sites of the (001) surface. For this purpose, we selected the anions O(11) at the center and O(31) at the corner of the standard cluster; the positions of all other ions of the standard cluster were kept fixed at values produced in rigid ion optimization of the slab model (see Fig. 2 and parameters set P1 in Table I). One should keep in mind that small structural distortions due to the combination of QM and MM treatments are inevitable; their correction is to some extent arbitrary. We intentionally have chosen to minimize such distortions, where possible, to achieve an improvement over schemes that employ geometry constraints; we adhere to this choice in a consistent fashion during the development of the EPE method.

In Step 1, the shell model⁶² yields in-plane and first interplane MgO nearest-neighbor distances for the ions of Region I at 2.104 and 2.098–2.106 Å, respectively (see Table

II). At this level of modeling, the rumpling (buckling) of the (001) surface (i.e., the distance between the planes of the top layer cations and anions) is below 0.01 Å. These values for the regular structure are to be compared with experimental nearest-neighbor distance of bulk MgO, 2.104 Å⁶⁸ as well as measured information of the rumpling of MgO(001), namely 0.02 ± 0.01 Å (GIXS)⁶⁹ or 0.11 ± 0.05 Å (LEED).⁷⁰ When only force-field correction terms of V_{nn}^{mod} (corresponding to parameter set P1) are applied with the geometry of the EPE region fixed (Step 2), the calculated geometry of the standard cluster exhibits notable distortions from both experimental and calculated references (see Table II). The rumpling of the top (001) layer is calculated at 0.044 or 0.008 Å since the oxygen anions in the center of cluster O(11) and in the corner positions are 2.156 and 2.120 Å above the second (001) crystallographic plane, respectively; in-plane nearest-neighbor distances that should be equal by translational symmetry differ by up to 0.046 Å, e.g., distances (12)–(22) and (22)–(52) (Table II). Apparently, force-field corrections due to V_{nn}^{mod} alone (parameter set P1) do not yield a local structure of a MgO cluster model that reflects the translational symmetry and the rumpling of the MgO(001) surface with sufficient accuracy.

Therefore, we decided to introduce further force-field correction terms V_{short} [see Eq. (3)], also of Buckingham type, for the interaction of the cations Mg^{2+} and $(Mg^{pp*})^{2+}$ with “shell-model” oxygen centers O_{sm} of Region IIa. As before, we compared potential energy curves for the displacement of these cations in [100] direction, both inside the QM cluster and at the boundary of the cluster with nearest neighbors in Region IIa (see parameter sets P2 in Table I). When both correction terms, V_{nn}^{mod} and V_{short} (parameter sets P1+P2) are applied, then we obtain a rather satisfactory equilibrium structure of the QM cluster model of the ideal O^{2-} site at the ideal MgO(001) surface. The resulting structure (see Table II and Fig. 2) constitutes the QM reference structure (Step 2) for the calculations of Step 3 (see Sec. II A). As major difference of this reference structure from the regular structure of Step 1, we note that interlayer nearest-

TABLE II. Effect of the force-field correction terms V_{nn}^{mod} and V_{short} for two parameter sets^a P1 and P2 on calculated distances Mg–O (in Å) between atoms $Mg(i_1j_1)$ and $O(i_2j_2)$ of the standard cluster $[O_8Mg_9]Mg_{16}^{pp*}$ modeling an O^{2-} site of the MgO(001) surface. The atom positions (i_kj_k) designate symmetry inequivalent positions i_k in the crystallographic (001) layer j_k of the cluster according to Fig. 2. For comparison, results for slab models of MgO obtained with the shell model and with a DF calculation are also shown.

	Atom pairs Mg–O									
	(12)	(21)	(32)	(21)	(21)	(41)	(12)	(32)	(52)	(23)
$Mg(i_1j_1)$	(12)	(21)	(32)	(21)	(21)	(41)	(12)	(32)	(52)	(23)
$O(i_2j_2)$	(11)	(22)	(31)	(11)	(31)	(31)	(22)	(22)	(22)	(22)
Slab, shell model ^b	2.106	2.098	2.106	2.104	2.104	2.104	2.104	2.104	2.104	2.122
Slab, DF ^c	2.106	2.072	2.106	2.090	2.090	2.090	2.090	2.090	2.090	2.086
EPE, P1 ^d	2.156	2.112	2.120	2.101	2.113	2.128	2.132	2.090	2.086	2.116
EPE, P1+P2 ^e	2.174	2.108	2.170	2.110	2.114	2.109	2.117	2.104	2.090	2.124

^aFor the values of the parameters, see Table I.

^bRegular structure (see Step 1); shell-model calculation on a slab model of six layers, intralayer nearest-neighbor distance fixed at the shell-model optimized value of bulk MgO, 2.104 Å.

^cPlane-wave LDA calculation [Ref. 16] on a slab model of seven layers, intralayer nearest-neighbor distance fixed at the optimized value of bulk MgO, 2.090 Å; Ref. 71.

^dQM/EPE (BP) calculation on the standard cluster with corrections due to V_{nn}^{mod} applied (for the parameter values, see Table I), V_{short} as in the shell model.

^eReference structure (Step 2) obtained by a QM/EPE(BP) calculation on the standard cluster with corrections due to V_{nn}^{mod} and V_{short} applied (for the parameter values, see Table I).

neighbor distances differ now typically by $\pm 0.01 \text{ \AA}$ [at most $\pm 0.03 \text{ \AA}$ for the distance (22)–(52); see Table II]. Thus, the translational (pseudo) symmetry of the whole structure is now reflected to a much better degree. Furthermore, with both correction terms applied, the rumpling of the top layer is clearly manifested. With about 0.06 \AA , it is slightly larger than the rumpling resulting from a full QM calculation on a seven-layer slab model,⁷¹ which yields 0.04 \AA , using the local density exchange-correlation approximation (LDA).⁷² This larger rumpling is also reflected by an elongation of the top interplane distance as measured by the bond lengths (11)–(12) and (31)–(32) which become equal, 2.17 \AA , with parameter set P1+P2 (see Table II and Fig. 2). These distances are somewhat longer, by 0.06 \AA , than in the QM slab model calculations. In this context it is important to note that a calculation on bulk MgO using a gradient-corrected exchange-correlation potential⁷³ yields an optimized nearest-neighbor distance of 2.132 \AA ⁷¹ which is by 0.03 \AA longer than in experiment⁶⁸ or in the shell model. As a consequence, the embedded QM cluster treated with the BP exchange-correlation approximation requires slightly more space than provided by the localizing potential well due to shell-model environment of the EPE approach. This small artifact seems acceptable as a consequence of the fact that two very different methods are used to describe Regions I and II in the EPE model. Finally, the fact that—at variance with the QM treatment—the shell-model description does not reproduce the rumpling of the MgO(001) surface of about 3% of the nearest-neighbor interior distance should be considered as a minor drawback of that model.

To calculate the EPE relaxation, the perturbing electrostatic potential due to the QM cluster was calculated using the fitted electron charge density representation of the LCGTO-FF-DF method.⁵¹ This is at variance with the ICE-CAP method²³ where a multipole expansion of the electron density of the cluster is used. In the present EPE calculations, convergence is achieved in a multilayer iteration process. In an “inner” loop, the EPE relaxation is iteratively determined for a fixed geometry of the QM cluster. For this purpose, after convergence of each Kohn–Sham procedure, a charge density fit is carried out which is then employed to relax the EPE.

For the resulting electrostatic potential of the EPE, the next Kohn–Sham procedure is performed and so on, until self-consistency is achieved as judged by the change of the total energy. Then, in the next step of an “outer” loop, at fixed EPE configuration, the cluster geometry is optimized using analytical energy gradients, to be followed by the next “inner” loop. This iteration process was stopped once the total energy of the whole system changed by less than $5 \times 10^{-5} \text{ eV}$; the same threshold is used for the “inner” and the “outer” loops.

III. RESULTS AND DISCUSSION

The growth of metal clusters and films on MgO support is often initiated at defect sites, in particular on surface vacancies of exposed (001) planes.^{74,75} The adsorption of isolated metal atoms on surface vacancies can be considered as the very first stage of metal deposition. An early quantum

chemical study of this step has been carried out for Rb, Pd, and Ag atoms using the Hartree–Fock (HF) self-consistent field method.^{26,76} Recently, the adsorption of Cu, Ni, Ag, and Pd atoms has been investigated with a gradient-corrected DF approach;³⁸ adsorption on both oxygen vacancies and regular O^{2-} centers of the MgO(001) surface has been considered. In this latter work, substrate model clusters embedded in a rigid matrix of pseudopotentials and PC’s were used which allowed to calculate a partial structural relaxation of the substrate.³⁸ To check the reliability of these simplified embedded cluster models, one needs a more accurate treatment of relaxation effects. In this vein, we have chosen the adsorption of single Pd atoms on regular O^{2-} sites and oxygen vacancies of the MgO(001) surface as the first application of the EPE embedding approach.

A. Oxygen vacancies on MgO(001)

Oxygen vacancies on the MgO(001) surface are well known for their ability to hold and donate electrons.⁹ The formation of F_s , F_s^+ , and F_s^{2+} surface defects formally corresponds to the removal of oxygen atoms, mono- and dianions, respectively, from the top layer of the substrate. An F_s site of MgO contains two electrons localized in the vacancy. The reactivity of these oxygen vacancy sites can be directly related to their ionization potentials and electronic affinities. We will see in the following that these characteristics are strongly affected by the structural relaxation of both a cluster model and its substrate environment.

In Table III we present calculated pertinent characteristics of unrelaxed and relaxed cluster models of the oxygen vacancies. In terms of displacements of the atoms closest to the vacancy, the relaxation is moderate for F_s and F_s^+ centers, but notably stronger for F_s^{2+} centers. For F_s the relaxation is essentially limited to displacements of the nearby Mg ions upward by 0.06 \AA and outward by 0.04 \AA . The oxygen atoms of the top MgO layer which are closest to the F_s vacancy are hardly shifted at all, by 0.01 \AA upward only. For F_s^+ centers, the displacement of Mg ions is somewhat larger, by 0.13 \AA outward and by 0.07 \AA upward (Table III). The oxygen cen-

TABLE III. Characteristics^a of unrelaxed (*u*) and relaxed (*r*) cluster models of oxygen vacancies F_s , F_s^+ , F_s^{2+} on MgO(001) calculated with the EPE approach.^b

	F_s		F_s^+		F_s^{2+}	
	<i>r</i>	<i>u</i>	<i>r</i>	<i>u</i>	<i>r</i>	
EA, eV		4.41	2.56(3.86)	9.86	4.52	
ΔE_r , eV	0.11 (0.11)		1.96(0.69)		7.30	
$\Delta r(\text{Mg})$, \AA	0.04		0.13		0.23	
$\Delta z(\text{Mg})$, \AA	0.06		0.07		0.06	
$\Delta r(\text{O})$, \AA	0.00		−0.07		−0.20	
$\Delta z(\text{O})$, \AA	0.01		0.07		0.14	

^aEA—electron affinity (calculated for an adiabatic change); Δr , Δz —displacements, in radial direction and normal to the surface, of the ions closest to the vacancy site in the “top layer” of the slab (a positive sign indicates an outward or upward shift, respectively); ΔE_r —relaxation energy. The values in parentheses are for the partially relaxed cluster models $\{[\text{O}_{12}\text{Mg}_9]^{6+}\}\text{Mg}_{40}^{pp*}$ (F_s) and $\{[\text{O}_{12}\text{Mg}_9]^{7+}\}\text{Mg}_{40}^{pp*}$ (F_s^+) of Ref. 38.

^bEmbedded cluster models $[\text{O}_8\text{Mg}_9]\text{Mg}_{16}^{pp*}$ (F_s), $\{[\text{O}_8\text{Mg}_9]\}^+\text{Mg}_{16}^{pp*}$ (F_s^+), and $\{[\text{O}_8\text{Mg}_9]^{2+}\}\text{Mg}_{16}^{pp*}$ (F_s^{2+}).

ters closest to the F_s^+ vacancy shift notably inward and upward, by 0.07 Å each. For F_s^{2+} centers, the calculated outward displacement of the Mg cations is substantial, 0.23 Å (Table III); simultaneously, these cations shift by 0.06 Å upward from their position at the ideal O^{2-} site. The closest oxygen anions of the top MgO layer also relax significantly, inward by 0.20 Å and upward by 0.14 Å. Apparently, the outward displacement of the Mg cations increases as the electron density in the vacancy is reduced, i.e., along the series $F_s \rightarrow F_s^+ \rightarrow F_s^{2+}$; thus, it changes as expected with the decreasing screening of the cation–cation repulsion. The anions behave differently. Because of their significantly larger size, the short-range repulsion is a more important factor for them. As the Pauli repulsion between the anionic and vacancy states decreases, the anions move inward with the tendency to occupy the volume spanned by the electrons trapped in the neutral vacancy.

The atomic displacements at F_s and F_s^+ centers calculated here using the EPE embedding scheme agree qualitatively with those obtained earlier when a constrained geometry relaxation was investigated.³⁸ There, the positions of the boundary PP centers and external PC's were kept fixed at the experimental bulk-terminated values. For instance, in that previous study the displacements of the Mg cations closest to the F_s^+ vacancy were calculated to 0.14 and 0.01 Å in outward and upward direction, respectively; these values are quite close to the present results (Table III).

The relaxation energies ΔE_r of the vacancy models, calculated as differences between total energies of the equilibrium structure of the O^{2-} regular site and the relaxed structure, are 0.11, 1.96, and 7.30 eV for F_s , F_s^+ , and F_s^{2+} , respectively (Table III). It is important to note that the relaxation significantly decreases the electron affinity (EA), here calculated adiabatically, as total energy differences at equilibrium, $EA(F_s^+) = E(F_s^+) - E(F_s)$ and $EA(F_s^{2+}) = E(F_s^{2+}) - E(F_s^+)$. For F_s^{2+} centers, the EA reduces from 9.86 to 4.52 eV. The EA value of an F_s^{2+} center without structural relaxation would suffice to oxidize a Pd atom which features a calculated ionization potential of 8.3 eV (in a BP description), 8.34 eV measured.⁷⁷ However, the electron affinity of a properly relaxed F_s^{2+} center renders a cationic state of an adsorbed Pd atom unlikely. Relaxation also decreases the electron affinity of an F_s^+ center, namely from 4.41 to 2.56 eV (Table III). The present EA result of an F_s^+ center is even lower than that obtained previously³⁸ with a partially relaxed cluster model, 3.86 eV (see Table III). Obviously, once the relaxation of the vacancy site is taken into account in an accurate fashion, e.g., as done by the present model study, a notable propensity for attracting electron density from adsorbed metal species exists only for F_s^{2+} centers.

The EA values of oxygen vacancies at the MgO(001) surface obtained with the EPE approach are very close to recent results calculated with clusters embedded in a $10 \times 10 \times 10$ ions cube of polarizable shell-model ions, namely 2.6 eV for F_s^+ centers and 4.5 eV for F_s^{2+} centers.⁹ Also, structural data determined in that study are very similar to the present results; there, the outward displacements of the Mg cations for F_s^+ and F_s^{2+} vacancies were calculated at 0.16 and 0.25 Å, respectively. Furthermore, the present results

show that an earlier investigation based on partially relaxed cluster models³⁸ was not completely successful in reproducing the effect of an elastic polarizable environment. This can be deduced from a comparison of the older results, given in Table III in parentheses, with the corresponding EPE values of the present study.

The description of optical transitions of F^+ centers of bulk MgO represented the first successful application of the method of self-consistent lattice polarization.¹¹ The Hartree–Fock energies of absorption and emission of F^+ centers, 4.95 and 3.27 eV, respectively, are in very good agreement with the measured values, 4.96 and 3.13 eV.¹¹ This model was also applied to structural relaxation of oxygen vacancies in bulk MgO. The formation energies of surface vacancies calculated here (Table III) are somewhat smaller and are in reasonable agreement with results of HF calculations on bulk F and F^+ centers using self-consistent embedding, $\Delta E_r(F) = 0.35$ eV and $\Delta E_r(F^+) = 2.76$ eV.¹¹ In those calculations, the lattice relaxation of an F^+ defect was characterized by outward displacements of the nearest-neighbor Mg cations by ~ 0.06 Å and by inward displacements of the nearest-neighbor O anions of the same amount. For neutral oxygen vacancies in the bulk which accommodate two electrons (F centers), both the nearest and next-nearest neighbors were calculated to relax inward by ~ 0.04 Å.

B. Adsorption of Pd atom on MgO(001)

We start the analysis of the results on the adsorption complexes with Pd on top of regular O^{2-} sites of MgO(001). Adsorption of various transition metal atoms has previously been modeled with cluster models embedded in PC arrays,^{36–38} but also with embedding by bare pseudopotentials³⁸ as well as with slab models.⁷⁹ With embedding in a simple PC array, the atoms of Cu, Ag, Au, Cr, and Mo were found to form relatively weak adsorption bonds, below 0.5 eV, whereas the atoms of Ni, Pd, Pt, and W are bound by about 1 eV or stronger.³⁶ In a more accurate approach with pseudopotentials at the cluster boundary, larger binding energies were calculated, by about 0.2 eV for the same exchange–correlation potential.³⁸ Thus far, in none of the computational investigations, was any evidence found for a notable charge transfer between the metal adsorbate and the regular MgO(001) substrate. It was concluded that polarization of the metal species in the electrostatic field of the surface and mixing of s and d_{z^2} orbitals of the metal atom with the $2p_z$ orbital of the surface oxygen ion constitute the two main contributions to the M–MgO(001) bonding. Evidently, the extent of the metal polarization and covalent mixing changes with the height of the metal atom above the surface.³⁸

To assess the sensitivity of the present results on methodical details, we compare calculated adsorption energies of a Pd atom at the regular O^{2-} site of MgO(001) as obtained with different variants of the QM/EPE cluster models. In Table IV we present adsorption energies calculated for clusters of different size, with and without inclusion of the BSSE corrections. We also investigated relativistic effects by comparing results of nonrelativistic and relativistic calculations; the latter have been carried out either with the scalar relativ-

TABLE IV. Binding energies (BE, in eV) of a Pd atom in adsorption complexes obtained with a nonrelativistic and relativistic DF treatment of various clusters^a modeling a regular O²⁻ site of the MgO(001) surface. The value BE(BSSE) indicates the binding energy corrected for the basis set superposition error. z(Pd-O) is Pd-O distance (in Å) at equilibrium.

		Nonrelativistic			Relativistic		
		BE	BE(BSSE)	z(Pd-O)	BE	BE(BSSE)	z(Pd-O)
1	Pd/[OMg ₅] ⁸⁺	-0.81	-0.80	2.21	-1.21	-1.17	2.11
2	Pd/[O ₉ Mg ₂₅] ³²⁺	-0.96	-0.94	2.19	-1.32	-1.26	2.11
3	Pd/[O] ²⁻ Mg ₅ ^{pp*}	-0.99	-0.79	2.18	-1.44	-1.22	2.04
4	Pd/[OO ₈ ^{pp} Mg ₉ ^{pp}]Mg ₁₆ ^{pp*}	-1.21	-0.97	2.21	-1.63	-1.35	2.11
5	Pd/[OO ₈ Mg ₉]Mg ₁₆ ^{pp*}	-0.96	-0.93	2.21	-1.35	-1.31	2.10
6	Pd ^{pp} /[O] ²⁻ Mg ₅ ^{pp*}				-1.47 ^b	-1.28 ^b	2.04 ^b
7	Pd ^{pp} /[OO ₈ ^{pp} Mg ₉ ^{pp}]Mg ₁₆ ^{pp*}				-1.68 ^b	-1.30 ^b	2.13 ^b
8	Pd ^{pp} /[OO ₈ Mg ₉]Mg ₁₆ ^{pp*}				-1.51 ^b	-1.27 ^b	2.13 ^b

^aAll cluster models treated by EPE embedding; geometry of the substrate fixed according to the regular structure (see Table II and Fig. 2).

^bRelativistic effects taken into account only via the (relativistic) effective core potential of Pd.

istic variant of the all-electron Douglas-Kroll-Hess approach to the Kohn-Sham problem⁵⁶ or with relativistic pseudopotentials for the Pd center.⁵⁷ In Table IV, we also compare data for cluster models of various degrees of sophistication: (i) models Pd/[OMg₅]⁸⁺ (**1**) and Pd/[O₉Mg₂₅]³²⁺ (**2**) with all oxygen centers surrounded in the first coordination sphere by regular cations, i.e., Mg²⁺ centers bearing basis functions, (ii) models Pd/[OMg₅^{pp*}]⁸⁺ (**3**) and Pd/[OO₈^{pp}Mg₉^{pp}]Mg₁₆^{pp*} (**4**) (corresponding to models **1** and **2**, respectively) where the first coordination sphere of the boundary oxygen atoms is represented by bare pseudopotentials (without basis functions). For highly ionic systems, both schemes of the cluster design are expected to furnish similar results. With deviations from the ideally ionic picture, these schemes tend to perform differently. Scheme (i) produces a more uniform distribution of the charge density around anions at the borders, but the cluster might acquire a somewhat electron deficit character because electron density can spread from the inner area of the cluster to its boundary Mg cations. Scheme (ii) with bare pseudopotentials (without basis functions) allows to utilize stoichiometric clusters, formally preventing artifacts where electron density is withdrawn at the cluster boundaries. However, the electron density distribution around the anions may become less uniform than in scheme (i).

As just mentioned, the study summarized in Table IV is devoted to various methodological aspects. In order to be able to compare various cluster models, their geometry has not been optimized. Rather, all calculations presented in Table IV have been performed at the geometries of substrate cluster that correspond to the equilibrium structure of the standard cluster [O₉Mg₉]Mg₁₆^{pp*} (Fig. 2 and Table II). Therefore, adsorption height and energy of Pd is derived from a limited optimization, taking into account only the height of the adsorbate above the top crystal plane. Later on, we shall discuss the consequences of substrate relaxation for the adsorption properties (see Table V).

Inspection of Table IV reveals that the Pd binding energy of the adsorption complexes Pd/(O²⁻)MgO depends only moderately on the way how the cluster boundary is repre-

sented. Even for cluster models of minimum size, **1** and **3**, substitution of the regular Mg cations by bare pseudopotential centers at the nonrelativistic level does not result in any significant change of the binding energy once the BSSE correction has been applied. The difference in the binding energies of models **1** and **3** at the relativistic level is calculated at 0.05 eV. As a side remark, we note that Mg²⁺ and Mg^{pp*} centers are not fully equivalent since the contribution of Mg^{pp*} centers are treated as an external potential, not subject to relativistic transformations.⁵⁶ The equilibrium height of the adsorbate above the surface oxygen atom changes appreciably between the two cluster models **1** and **3**; if the centers Mg²⁺ at the cluster “borders” are replaced by bare pseudopotential centers (Mg^{pp*})²⁺, then the pertinent bond distance decreases by 0.03 Å in the nonrelativistic and by 0.07 Å in the relativistic calculation.

Cluster-size effects are rather limited for the systems under consideration. Ongoing from the minimum all-electron cluster Pd/[OMg₅]⁸⁺ (**1**) to the extended model Pd/[O₉Mg₂₅]³²⁺ (**2**), the BSSE corrected binding energy (BE) of the adsorbate changes by less than 0.15 eV, at both the nonrelativistic and the relativistic level of calculations. Next, we compare the results of models **2**, **4**, and **5** which are of equal size, but feature different representations of the substrate centers: **2**—an all-electron description, **4**—an almost complete pseudopotential description (with bare pseudopotentials for the 16 cations at the cluster boundary), and the “standard” cluster **5**. Within each series, nonrelativistic or relativistic, essentially the same value is obtained for the adsorption height (Table IV), with one exception, namely the nonrelativistic calculations on **2** yields a slightly shorter value, by 0.02 Å. Also the binding energy shows little variation, 0.04 eV within the nonrelativistic series and 0.09 eV within the relativistic series.

Relativistic effects considerably increase the adsorption energy of Pd on the ideal O²⁻ site of the MgO(001) surface, by about 0.35 eV. In detail, the BE value increases by 0.37, 0.43, 0.30, 0.38, and 0.37 eV for the minimum cluster models Pd/[OMg₅]⁸⁺ (**1**) and Pd/[OMg₅^{pp*}]⁸⁺ (**3**) and the extended cluster models Pd/[O₉Mg₂₅]³²⁺ (**2**)

TABLE V. Calculated characteristics^a of adsorption complexes of Pd atoms at the regular O²⁻ site and at oxygen vacancies of the MgO(001) surface calculated with unrelaxed (*u*) and relaxed (*r*) EPE cluster models.^b Also shown are results of an earlier investigation^c with embedding in a finite array (FA) of bare pseudopotential centers and point charges.

		O ²⁻		F _s		F _s ⁺		F _s ²⁺
		EPE	FA ^d	EPE	FA ^d	EPE	FA ^d	EPE
BE, eV	<i>u</i>	-1.31	-1.35	-3.63	-3.76	-2.58	-2.62	-2.25
	<i>r</i>	-1.42		-4.02	-3.90	-2.53	-2.59	-1.31
z(Pd-Mg ₄), Å	<i>u</i>	2.17 ^e	2.11	1.51	1.53	1.59	1.61	1.60
	<i>r</i>	2.12 ^f		1.48	1.51	1.54	1.49	1.53
Δr(Mg), Å	<i>r</i>	0.04		0.04		0.02		-0.03
Δz(Mg), Å	<i>r</i>	0.05		0.02		0.02		-0.01
Δr(O), Å	<i>r</i>	0.01		0.04		0.04		0.04
Δz(O), Å	<i>r</i>	0.00		0.00		-0.02		0.00
∂μ/∂z, au	<i>u</i>	0.02	-0.02	-0.51	-0.45	-0.10	-0.05	0.27
	<i>r</i>	0.03		-0.59		-0.28		0.00

^aBE—adsorption energy, z(Pd-Mg₄)—equilibrium height of the adsorbate above the plane defined by the four nearest-neighbor Mg centers, Δr, Δz—displacements, in radial direction and normal to the surface, of the ions closest to the vacancy site in the “top layer” of the slab (a positive sign indicates an outward or upward shift, respectively), ∂μ/∂z—dipole moment derivative with respect to the vertical displacement z of the adsorbate at equilibrium.

^bSubstrate fully relaxed (*r*) modeled by the EPE embedded standard cluster model {[O₈Mg₉]^{q+}}Mg₁₆^{pp*} (*q*=0,1,2), unrelaxed substrate (*u*) as in the regular structure (Step 2).

^cUnrelaxed substrate structure (*u*) as in bulk-terminated MgO; the partially relaxed structure (*r*) refers to a model of the (free) vacancy site where the positions of the four oxygen centers closest to the vacancy were optimized and then kept fixed in the Pd adsorption complex; for details see Ref. 38.

^dFrom Ref. 38.

^ez(Pd-O)=2.10 Å.

^fz(Pd-O)=2.08 Å.

Pd/[OO₈^{pp}Mg₉^{pp}]Mg₁₆^{pp*} (**4**), and Pd/[OO₈Mg₉]Mg₁₆^{pp*} (**5**), respectively. For the standard cluster **5**, the binding energy increases by 40% on going from a nonrelativistic to a relativistic description. Evidently, these data are at variance with the point of view that for 4*d* transition metals relativistic effects are always moderate; of course, other examples are known, too.⁸⁰ In any case, for the standard cluster **5**, we calculate an adsorption height of 2.10 Å and a binding energy of 1.31 eV. This latter value is in good agreement with the result of our previous, simpler model description³⁸ where an adsorption height of 2.11 Å and an adsorption energy of 1.35 eV had been calculated.

Finally, we turn to a discussion of the relativistic effects as described by a pseudopotential treatment of the “heavy element” Pd. This has been probed for three models **6**, **7**, and **8** which correspond to models **3**, **4**, and **5**, respectively (Table IV). Over all, adsorption height and binding energy, calculated for the “pseudopotential” models, compare satisfactorily with the results of the corresponding model that features an all-electron description of the Pd center; binding energy values differ by at most 0.06 eV (for the minimum models **3** and **6**). For the standard clusters **5** and **8** we note an extension of the Pd-O bond by 0.02 Å and a decrease of the binding energy by 0.03 eV when Pd is described by a pseudopotential.

Next we shall discuss the adsorption of Pd at regular oxygen sites of the MgO(001) surface and at various oxygen vacancies when the relaxation of the substrate is fully taken into account (see Fig. 3). Pertinent parameters of Pd adsorption complexes at the regular O²⁻ center and at the oxygen vacancies F_s, F_s⁺, and F_s²⁺ are given in Table V. We compare calculated results at equilibrium (*r*—relaxed) to those where all substrate centers were kept fixed at their positions calculated for the regular O²⁻ site (*u*—unrelaxed; see com-

plex **5** of Table IV); in the latter case, only one degree of freedom was optimized, the adsorption height of Pd.

Relaxation effects of the EPE embedded models increase (the absolute values of) the energy of adsorption (BE) at the sites O²⁻ by 0.11 eV to BE=-1.42 eV, while the adsorption height z (above the plane of the four nearest-neighbor Mg

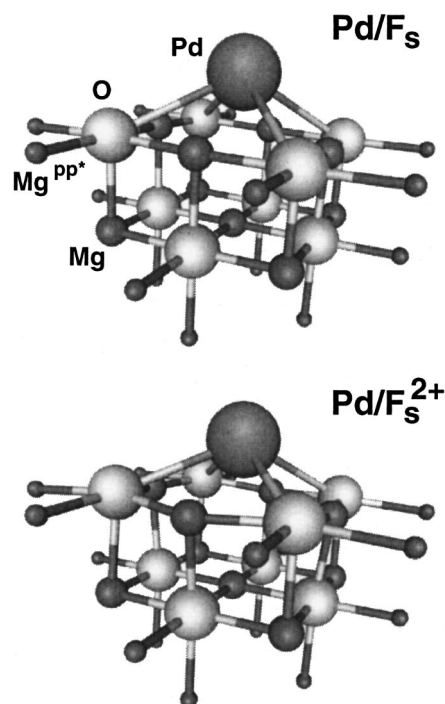


FIG. 3. Sketch of the optimized structure of the adsorption complexes Pd/F_s and Pd/F_s²⁺ as obtained from an EPE cluster model calculation. Layout as in Fig. 2.

centers) decreases by 0.05 Å as these Mg centers on relaxation are shifted up 0.05 Å. The almost negligible values of dipole moment derivative $\partial\mu/\partial z$ of the system with respect to the vertical displacement of Pd atom (taken at the equilibrium position) indicate that the adsorption at the regular site O^{2-} does not ensue any notable charge transfer between adsorbate and substrate.^{13,38} With grazing incidence x-ray spectroscopy, the Pd– O^{2-} distance at the Pd/MgO(001) interface was determined to 2.216 ± 0.02 Å.⁸¹ This value is larger than the one calculated with our model (Table V), partly because the distance is coverage dependent; it is expected to be shorter in the zero-coverage limit.^{39,40} For instance, the Pd–O distance for Pd₄/MgO(001) was calculated at 2.24 Å in very good agreement with experiment.⁴⁰ Recently, nucleation and growth of Pd on MgO(001) have been studied by variable-temperature atomic force microscopy.⁸² From these experiments the adsorption energy of a single Pd atom at regular sites of MgO(001) terraces was estimated to -1.2 ± 0.2 eV, in satisfactory agreement with the present calculated value, -1.42 eV.

By far the strongest adsorbate–substrate interaction among the four adsorption complexes investigated (Table V) occurs for the neutral oxygen vacancy F_s . The large adsorption energy of the unrelaxed complex increases even further, by 0.39 eV, to $BE = -4.02$ eV when the relaxation of the substrate is taken into account. Energy is gained, 0.12 eV, as compared to the case when relaxation is taken into account only partially where only the four oxygen atoms closest to the vacancy were allowed to relax in the free substrate and relaxation of substrate was not permitted after deposition of the metal atom.³⁸ In the present study the energy gain with respect to Pd adsorption on the F_s site frozen at its relaxed structure ($BE = -3.84$ eV) is 0.18 eV, i.e., half of the overall (absolute) binding energy increase due to the complete relaxation. In both the present and previous³⁸ calculations, relaxation increases the stability of the adsorption complex Pd/ F_s ; the relaxation energy in the final state with the electron density donated to Pd is larger than that for the initial state of an isolated F_s center. The relaxation of the F_s center is accompanied by a donation of the electron density to Pd atom as indicated by the negative value of the dipole moment derivative, $\partial\mu/\partial z = -0.59$ au. This is a rather large value for a metal atom adsorbed at MgO(001). Therefore, it is not surprising that the charge redistribution causes a relaxation that is larger than in the case of a neutral F_s center without the Pd adsorbate. While the structural relaxation of the Pd/ F_s adsorption complex is important for an accurate determination of the metal binding energy, its direct effect on the height of Pd above the surface is very small; the adsorption height z changes from 1.51 to 1.48 Å (Table V). Due to substrate relaxation after Pd adsorption, the four cations closest to the Pd atom move outward and upward by 0.04 and 0.02 Å, respectively. Also the nearest anions move slightly outward. The resulting substrate structure exhibits a much reduced rumpling in the vicinity of the adsorption site.

For the adsorption complex Pd/ F_s^+ at the singly charged oxygen vacancy, substrate relaxation slightly affects the binding energy, confirming earlier findings with a model based on partial substrate relaxation.³⁸ In the present calcu-

lations the energy is reduced by 0.05 eV; previously, we had found a lowering of the binding energy by 0.03 eV.³⁸ Compared to the complex Pd/ F_s at the neutral vacancy, relaxation affects the adsorption height somewhat stronger. The adsorption height is reduced from 1.59 to 1.54 Å (Table V); this reduction is notably smaller than in the previous work where a reduction of the adsorption height, from 1.61 to 1.49 Å, had been calculated.³⁸ The formation of the Pd/ F_s^+ adsorption complex results in small displacements of the neighboring atoms; cation and anions move outward by at most 0.04 Å and the cations undergo an additional upward displacement by 0.02 Å. A fully relaxed F_s^+ center donates electronic charge density more readily to an adsorbed Pd atom, as indicated by the dynamic dipole moment $\partial\mu/\partial z = -0.28$ au; this value is notably larger (by absolute value) than that computed for the adsorption complex without relaxation,³⁸ -0.05 au. From the Arrhenius representation of the Pd island density measured by variable-temperature atomic force microscopy and fitted with a rate equation model, the absolute value of the interaction energy of a Pd atom with unidentified point defects on the MgO(001) surface was estimated to at least 2.4 eV, with the best fit obtained at 2.7 eV.⁸² These values are close to the calculated desorption energy for Pd on F_s^+ site, 2.53 eV, but considerably lower than the value calculated for F_s centers, 4.02 eV, which trap Pd atoms most strongly.

Finally, we discuss the adsorption complex Pd/ F_s^{2+} (Fig. 3). Here, the energy effect of the substrate relaxation is dramatically different. The binding energy decreases by 0.94 eV to -1.31 eV, because of a strong relaxation of the initial state (Table V). Concomitantly, the adsorption height shrinks from 1.60 to 1.53 Å. On Pd adsorption the four cations closest to the vacancy shift inward and downward; on the other hand, the four closest anions exhibit an outward shift as in all other Pd adsorption complexes, here by 0.04 Å. An adsorption complex with a doubly-charged F_s^{2+} center may be considered as limiting case for estimating the oxidizing power of the oxide substrate under study. Such a vacancy site belongs to the kind of structural defects reminiscent of low-coordinated surface cations. Even in this limiting case no transfer of electron density from Pd to substrate is calculated, as indicated by $\partial\mu/\partial z = 0.00$ au (Table V). As judged by its interaction with a Pd atom, an F_s^{2+} center exhibits certain similarities to a regular O^{2-} center. Compared to adsorption at the nonpolar (001) surface, adsorption on polar surfaces of MgO may be expected to result in a more ionic bonding. From the present results for Pd adsorption on an F_s^{2+} defect, a system with a large electron affinity, we anticipate that isolated noble metal atoms also will not be oxidized by interaction with *relaxed* polar surfaces of MgO. Indeed, we have seen that the relaxation of an F_s^{2+} defect leads to a dramatic reduction of EA; one expects this to be a general feature of ionic oxide materials. This expectation is in line with recently calculated data for Ag/MgO(110)⁸³ (periodic HF calculations with *a posteriori* DF exchange–correlation corrections) and Pd/ α -Al₂O₃(0001) (DF EPE embedded cluster calculations⁸⁴) where no indication of ionic bonding with d^{10} metal atoms was found.

The EPE model consistently accounts for relaxation and

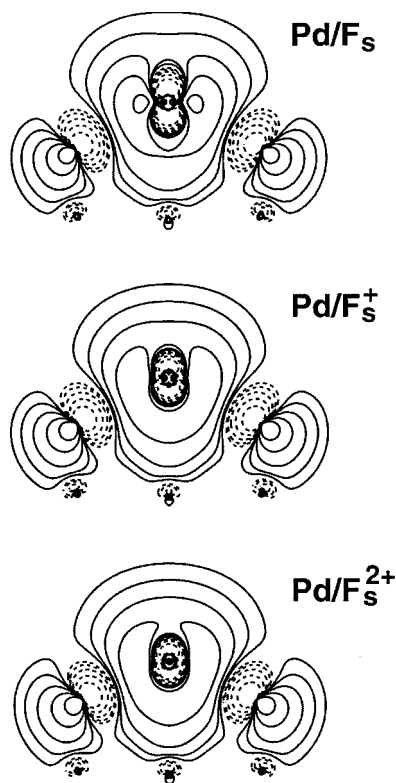


FIG. 4. Contour plots of MO $29a_1$, which forms the HOMO of Pd/F_s , the singly occupied MO (SOMO) of Pd/F_s^+ , and the LUMO of $\text{Pd}/\text{F}_s^{2+}$. The orbital is shown in the vertical (110) plane; cf. Fig. 2. The contour values are 0.08, 0.04, 0.02, 0.01, and 0.005 au; solid and dashed lines indicate values of opposite sign.

it provides significant corrections to various adsorption properties, in particular to adsorption energies and dynamic dipole moments. Yet, there is no qualitative change of the picture of the adsorption interaction as compared to our previous study which took only a partial relaxation of the substrate into account.³⁸ In the adsorption complex $\text{Pd}/\text{F}_s^{2+}$, the bonding orbital $29a_1$ formed from the LUMO of the doubly charged vacancy site (or the HOMO of the sites F_s^+ and F_s) and the valence s orbital of the Pd atom is empty (Fig. 4). In the corresponding complexes with F_s^+ and F_s centers, this orbital is occupied by one and two electrons, respectively. This results in the energy gain of 1.2–1.5 eV per electron occupying this bonding orbital: the binding energy is calculated to ~ 2.5 eV for the adsorption complexes Pd/F_s^+ and ~ 4.0 eV for Pd/F_s (Table V).

A further trend along the series $\text{F}_s \rightarrow \text{F}_s^+ \rightarrow \text{F}_s^{2+}$ reflects a gradual change of the character of the adsorbate–substrate bonding. The calculated adsorbate binding energy follows a perfect linear correlation with the dynamic dipole moment $\partial\mu/\partial z$ at equilibrium which provides a measure of the charge redistribution upon adsorption, $\text{BE}/\text{eV} = -1.29 + 4.60 \partial\mu/\partial z/\text{au}$, with $r^2 = 1.000$. Even with the values of the ideal site O^{2-} included, the correlation remains very good: $\text{BE}/\text{eV} = -1.41 + 4.34 \partial\mu/\partial z/\text{au}$, with $r^2 = 0.996$. In line with earlier findings,³⁸ these new correlations reflect a notable polar covalent contribution to the adsorption bond of Pd at F_s and F_s^+ , increasing from $\text{Pd}/\text{F}_s^{2+}$ to Pd/F_s^+ and to Pd/F_s . Indeed, the gradual occupation of MO $29a_1$ causes

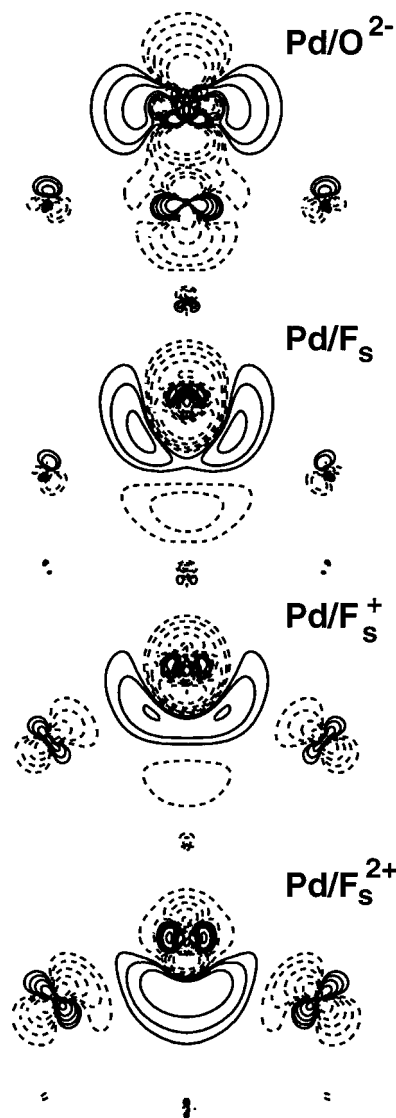


FIG. 5. Electron density difference plots for $\text{Pd}/\text{F}_s^{q+}$: $\Delta\rho(\text{Pd}/\text{F}_s^{q+}) = \rho(\text{Pd}/\text{F}_s^{q+}) - \rho(\text{Pd}) - \rho(\text{F}_s^{q+})$ shown in the vertical (110) plane containing the Pd atom. The contour values are 0.02, 0.01, 0.005, 0.0025, and 0.001 25 au; dashed lines indicate negative values.

electron density to be withdrawn from the vacancy; it is effectively donated into the Pd $5s$ orbital. This donation effect is proportional to the MO occupation numbers one (Pd/F_s^+) or two (Pd/F_s) because the shape of the orbital $29a_1$ in the species $\text{Pd}/\text{F}_s^{2+}$, Pd/F_s^+ , and Pd/F_s remains essentially unchanged (Fig. 4), notwithstanding the mutual atom displacements being particularly notable in $\text{Pd}/\text{F}_s^{2+}$. This interaction mechanism is supported by the significant increase of the Pd $5s$ Mulliken population which changes from 0.42 to 1.10 to 1.66 au for $\text{Pd}/\text{F}_s^{2+}$, Pd/F_s^+ , and Pd/F_s , respectively, whereas the Pd $4d$ population remains almost constant, 9.61, 9.56, and 9.46 au, respectively. More reliable than a Mulliken population analysis (especially for the case of extended basis sets used here) is a visualization of the charge density differences displayed in Fig. 5. These plots demonstrate increased electron density in closer and closer vicinity of the Pd atom for $\text{Pd}/\text{F}_s^{2+}$, Pd/F_s^+ , and Pd/F_s ; this charge rearrangement is accompanied by increasing (absolute) values of

the binding energy of 1.2–1.5 eV per additional electron (Table V). The binding energy offset of ~ 1.3 – 1.4 eV calculated for $\text{Pd}/\text{F}_s^{2+}$ and Pd/O^{2-} is also present in the adsorption complexes Pd/F_s^+ and Pd/F_s ; it can be assigned to the polarization of a Pd atom adsorbed at the $\text{MgO}(001)$ surface.

IV. CONCLUSIONS

In this work, we have introduced a variational procedure that permits a flexible and consistent embedding of cluster models in a classical atomistic environment for the description of surfaces of ionic systems. Reflecting on the specifics of this embedding formalism, it is referred to as *elastic polarizable environment*, EPE. This procedure has been implemented in the parallel density functional code PARAGAUSS. Adsorption of single Pd atoms on F_s , F_s^+ , and F_s^{2+} defect sites as well as on the regular O^{2-} site of the $\text{MgO}(001)$ surface was studied computationally. The effects of the lattice relaxation around the cluster in response to both the formation of a defect and the charge transfer between the substrate and the adsorbate have been considered. This work complements and extends our previous first-principles cluster calculations on metal particles interacting with the $\text{MgO}(001)$ surface.^{36,38,39,78}

Of the three examined vacancy sites, F_s^{2+} , F_s^+ , and F_s , the properties with respect to Pd atom adsorption of the first one, F_s^{2+} , are most similar to those of a regular O^{2-} site of the $\text{MgO}(001)$ surface. In neither $\text{Pd}/\text{F}_s^{2+}$ nor Pd/O^{2-} appreciable electron density donation to or from the substrate has been found; the bonding in $\text{Pd}/\text{F}_s^{2+}$ is mainly caused by polarization of the metal in the electrostatic field of the strongly relaxed substrate. The binding energies of the complexes $\text{Pd}/\text{F}_s^{2+}$ and Pd/O^{2-} are calculated at -1.31 and -1.42 eV, respectively. On going from F_s^{2+} to F_s^+ and F_s , the binding energy increases when the bonding orbital formed by the HOMO of the defect and the valence s -orbital of the adsorbate is filled by one or two electrons, reaching about -2.5 and -4.0 eV, respectively.

Relaxation of the substrate from the bulk terminated or the proper surface geometry results in a significant quantitative changes of calculated observables for the vacancy centers and their adsorption complexes. The electron affinity decreases due to the relaxation by about 1.9 and 5.3 eV for F_s^+ and F_s^{2+} centers, respectively. Such large changes certainly affect the relative weights of ionic and covalent contributions to the chemical bonding between the defect substrate and an adsorbed metal atom. As a consequence of the relaxation, more electron density trapped at the vacancy is donated to the adsorbed Pd atom. Concomitant to the charge redistribution in the adsorption complex Pd/F_s (manifested by increased value of $\partial\mu/\partial z = -0.59$ au) and the subsequent relaxation, the binding energy increases by about 0.4 eV. On the other hand, the binding energy of the adsorption complex $\text{Pd}/\text{F}_s^{2+}$ is reduced by about 1.0 eV upon substrate relaxation. Instead of an ionic bond with an oxidized Pd atom which might be expected from the electron affinity of an unrelaxed F_s^{2+} center, an unpolar character is determined for the adsorption bond.

ACKNOWLEDGMENTS

The authors thank W. Alsheimer, R. Kosarev, S. Krüger, A. Matveev, and I. Yudanov for fruitful discussions and help with test calculations. This work has been supported by Volkswagen Stiftung (Grant I/73653), INTAS/RFBR (Grant IR-97-1071/RFBR 97-03-71057), Krasnoyarsk Regional Scientific Foundation (Grants No. 1F0161, 6F0151), Deutsche Forschungsgemeinschaft, and the Fonds der Chemischen Industrie.

- ¹ *Cluster Models for Surface and Bulk Phenomena*, NATO ASI series B, Vol. 283, edited by G. Pacchioni, P. S. Bagus, and F. Parmigiani (Plenum, New York, 1992).
- ² U. Gutdeutsch, U. Birkenheuer, and N. Rösch, *J. Chem. Phys.* **109**, 2056 (1998).
- ³ M. Sierka and J. Sauer, *Faraday Discuss.* **106**, 41 (1997).
- ⁴ M. W. Deem, J. M. Newsam, and S. K. Sinha, *J. Phys. Chem.* **94**, 8356 (1990).
- ⁵ C. R. A. Catlow, D. H. Gay, M. A. Nygren, and D. C. Sayle, in *Chemisorption and Reactivity on Supported Clusters and Thin Films*, NATO ASI Series E, Vol. 331, edited by R. Lambert and G. Pacchioni (Kluwer, Dordrecht, 1997), pp. 479–521.
- ⁶ J. Gao, in *Review in Computational Chemistry* (VCH, New York, 1995), Vol. 7, pp. 119–185.
- ⁷ P. Sherwood, A. H. deVries, S. J. Collins, S. P. Greatbanks, N. A. Burton, M. A. Vincent, and I. H. Hillier, *Faraday Discuss.* **106**, 79 (1997).
- ⁸ R. B. Murphy, D. M. Philipp, and R. A. Friesner, *Chem. Phys. Lett.* **321**, 113 (2000).
- ⁹ P. V. Sushko, A. L. Shluger, and C. R. A. Catlow, *Surf. Sci.* **450**, 153 (2000).
- ¹⁰ N. Rösch, U. Birkenheuer, G. N. Vayssilov, V. A. Nasluzov, K. M. Neyman, S. Krüger, and M. Fuchs (unpublished).
- ¹¹ J. M. Vail, *J. Phys. Chem. Solids* **51**, 589 (1990).
- ¹² Z. Barandiarán and L. Seijo, *J. Chem. Phys.* **89**, 5739 (1988).
- ¹³ I. V. Yudanov, V. A. Nasluzov, K. M. Neyman, and N. Rösch, *Int. J. Quantum Chem.* **65**, 976 (1997).
- ¹⁴ L. Pettersson, M. Nyberg, J.-L. Pascual, and M. Nygren, in *Chemisorption and Reactivity of Supported Clusters and Thin Films*, NATO ASI Series E, Vol. 331, edited by R. Lambert and G. Pacchioni (Kluwer, Dordrecht, 1997), pp. 425–45.
- ¹⁵ J. M. Wittbrodt, W. L. Hase, and H. B. Schlegel, *J. Phys. Chem. B* **102**, 6539 (1998).
- ¹⁶ G. Kresse and J. Hafner, *Phys. Rev. B* **47**, 558 (1993); **49**, 14251 (1994); **54**, 11169 (1996).
- ¹⁷ G. Galli and M. Parrinello, in *Computer Simulation in Materials Science*, NATO ASI series E, Vol. 205, edited by M. Mayer and V. Pontikis (Kluwer Academic, Dordrecht, 1991), p. 283.
- ¹⁸ C. R. A. Catlow and W. C. Mackrodt, in *Computer Simulation of Solids*, Lecture Notes in Physics, Vol. 166, edited by C. R. A. Catlow and W. C. Mackrodt (Springer, Berlin, 1982), p. 3.
- ¹⁹ A. L. Shluger and J. D. Gale, *Phys. Rev. B* **54**, 962 (1996).
- ²⁰ A. B. Lidiard, *J. Chem. Soc., Faraday Trans. 2* **85**, 341 (1989).
- ²¹ E. V. Stefanovich and T. N. Truong, *J. Chem. Phys.* **102**, 5071 (1995).
- ²² B. G. Dick and A. W. Overhauser, *Phys. Rev.* **112**, 90 (1958).
- ²³ J. H. Harding, A. H. Harker, P. B. Keegstra, R. Pandey, J. M. Vail, and C. Woodward, *Physica B & C* **131**, 151 (1985).
- ²⁴ J. M. Vail, R. Pandey, and A. B. Kunz, *Rev. Solid State Sci.* **5**, 181 (1991).
- ²⁵ V. E. Puchin, E. V. Stefanovich, and T. N. Truong, *Chem. Phys. Lett.* **304**, 258 (1999).
- ²⁶ A. M. Ferrari and G. Pacchioni, *J. Phys. Chem.* **100**, 9032 (1996).
- ²⁷ M. A. Nygren, L. G. M. Pettersson, Z. Barandiarán, and L. Seijo, *J. Phys. Chem.* **100**, 2010 (1994).
- ²⁸ N. W. Winter, R. M. Pitzer, and D. K. Temple, *J. Chem. Phys.* **86**, 3549 (1987).
- ²⁹ V. A. Nasluzov, G. L. Gutsev, V. V. Rivanenkov, K. M. Neyman, and A. G. Anshits, *Soviet J. Struct. Chem.* **33**, 157 (1992).
- ³⁰ M. A. Nygren and L. G. M. Pettersson, *J. Chem. Phys.* **105**, 9339 (1996).
- ³¹ W. H. Adams, *J. Chem. Phys.* **37**, 2009 (1962).
- ³² T. L. Gilbert, *J. Chem. Phys.* **60**, 3835 (1974).
- ³³ A. B. Kunz and D. L. Klein, *Phys. Rev. B* **17**, 4614 (1978).
- ³⁴ A. B. Kunz and J. M. Vail, *Phys. Rev. B* **38**, 1058 (1988).

- ³⁵T. Belling, T. Grauschopf, S. Krüger, M. Mayer, F. Nörtemann, M. Staufer, C. Zenger, and N. Rösch, in *High Performance Scientific and Engineering Computing*, Vol. 8, Lecture Notes in Computational Science and Engineering, edited by H.-J. Bungartz, F. Durst, and C. Zenger (Springer, Heidelberg, 1999) p. 439.
- ³⁶I. Yudanov, G. Pacchioni, K. Neyman, and N. Rösch, *J. Phys. Chem. B* **101**, 2786 (1997).
- ³⁷K. M. Neyman, S. Vent, G. Pacchioni, and N. Rösch, *Nuovo Cimento D* **19**, 1743 (1997).
- ³⁸A. V. Matveev, K. M. Neyman, I. V. Yudanov, and N. Rösch, *Surf. Sci.* **426**, 123 (1999).
- ³⁹A. V. Matveev, K. M. Neyman, G. Pacchioni, and N. Rösch, *Chem. Phys. Lett.* **299**, 603 (1999).
- ⁴⁰A. M. Ferrari, C. Xiao, K. M. Neyman, G. Pacchioni, and N. Rösch, *Phys. Chem. Chem. Phys.* **1**, 4655 (1999).
- ⁴¹J. F. Goellner, K. M. Neyman, M. Mayer, F. Nörtemann, B. C. Gates, and N. Rösch, *Langmuir* **16**, 2736 (2000).
- ⁴²A. M. Ferrari and G. Pacchioni, *J. Phys. Chem.* **99**, 17010 (1995).
- ⁴³M. Bäumer and H.-J. Freund, *Prog. Surf. Sci.* **61**, 127 (1999).
- ⁴⁴A. Yu. Stakheev and L. M. Kustov, *Appl. Catal., A* **188**, 3 (1999).
- ⁴⁵N. F. Mott and M. J. Littleton, *Trans. Faraday Soc.* **34**, 485 (1938).
- ⁴⁶R. W. Grimes, C. R. A. Catlow, and A. M. Stoneham, *J. Phys.: Condens. Matter* **1**, 7367 (1989).
- ⁴⁷Y. Zhang, T.-S. Lee, and W. Yang, *J. Chem. Phys.* **110**, 46 (1999).
- ⁴⁸C. Noguera, A. Pojani, F. Finocchi, and J. Goniakowski, in *Chemisorption and Reactivity on Supported Clusters and Thin Films*, NATO ASI Series E, Vol. 331, edited by R. Lambert and G. Pacchioni (Kluwer, Dordrecht, 1997), p. 455.
- ⁴⁹R. Pandey, J. Zuo, and A. B. Kunz, *J. Mater. Res.* **5**, 623 (1990).
- ⁵⁰H.-J. Freund, *Faraday Discuss.* **114**, 1 (1999).
- ⁵¹B. I. Dunlap and N. Rösch, *Adv. Quantum Chem.* **21**, 317 (1990).
- ⁵²T. Belling, T. Grauschopf, S. Krüger, F. Nörtemann, M. Staufer, M. Mayer, V. A. Nasluzov, U. Birkenheuer, A. Hu, A. V. Matveev, and N. Rösch, *PARA GAUSS 2.1* (Technische Universität München, 1999).
- ⁵³A. D. Becke, *Phys. Rev. A* **38**, 3098 (1988).
- ⁵⁴J. P. Perdew, *Phys. Rev. B* **33**, 8822 (1986); erratum, **34**, 7406 (1986).
- ⁵⁵O. D. Häberlen and N. Rösch, *Chem. Phys. Lett.* **199**, 491 (1992).
- ⁵⁶N. Rösch, S. Krüger, M. Mayer, and V. A. Nasluzov, in *Recent Developments and Applications of Modern Density Functional Theory*, edited by J. Seminario (Elsevier, Amsterdam, 1996), Vol. 4, pp. 497–566.
- ⁵⁷P. J. Hay and W. R. Wadt, *J. Chem. Phys.* **82**, 270 (1985).
- ⁵⁸A. Hu, M. Staufer, U. Birkenheuer, V. Igoshine, and N. Rösch, *Int. J. Quantum Chem.* **79**, 209 (2000).
- ⁵⁹A. Bergner, M. Dolg, W. Küchle, H. Stoll, and H. Preuss, *Mol. Phys.* **80**, 1431 (1993).
- ⁶⁰P. Fuentealba, L. V. Szentpaly, M. Preuss, and M. Stoll, *J. Phys. B* **18**, 1287 (1985).
- ⁶¹S. F. Boys and F. Bernardi, *Mol. Phys.* **19**, 553 (1970).
- ⁶²G. V. Lewis and C. R. A. Catlow, *J. Phys. C* **18**, 1149 (1985).
- ⁶³U. Birkenheuer, J. C. Boettger, and N. Rösch, *J. Chem. Phys.* **100**, 6826 (1994).
- ⁶⁴D. E. Parry, *Surf. Sci.* **49**, 433 (1975); erratum, **54**, 195 (1976).
- ⁶⁵E. V. Stefanovich and T. N. Truong, *J. Phys. Chem. B* **102**, 3018 (1998).
- ⁶⁶V. I. Lebedev, *J. Comput. Math. Phys.* **15**, 48 (1975).
- ⁶⁷M. Sangster and A. Stoneham, *Philos. Mag. B* **43**, 597 (1981).
- ⁶⁸R. W. G. Wyckoff, *Crystal Structures*, 2nd ed. (Interscience, New York, 1963) Vol. 1.
- ⁶⁹O. Robach, G. Renaud, and A. Barbier, *Surf. Sci.* **401**, 227 (1998).
- ⁷⁰D. L. Blanchard, D. L. Lessor, J. P. LaFemina, D. R. Baer, B. W. K. Ford, and T. Guo, *J. Vac. Sci. Technol. A* **9**, 1814 (1991).
- ⁷¹W. Alsheimer, S. Krüger, and N. Rösch (unpublished).
- ⁷²S. H. Vosko, L. Wilk, and M. Nusair, *Can. J. Phys.* **58**, 1200 (1980).
- ⁷³J. P. Perdew, J. A. Chevary, S. H. Vosko, K. A. Jackson, M. R. Pederson, D. J. Singh, and C. Fiolhais, *Phys. Rev. B* **46**, 6671 (1992).
- ⁷⁴M. Meunier and C. R. Henry, *Surf. Sci.* **307–309**, 587 (1994).
- ⁷⁵I. Alstrup and P. J. Møller, *Appl. Surf. Sci.* **33–34**, 143 (1988).
- ⁷⁶N. Rösch and G. Pacchioni, in *Chemisorption and Reactivity of Supported Clusters and Thin Films*, NATO ASI Series E, Vol. 331, edited by R. Lambert and G. Pacchioni (Kluwer, Dordrecht, 1997), p. 395.
- ⁷⁷*Periodensystem der Elemente* (VCH, Weinheim, 1995).
- ⁷⁸I. V. Yudanov, S. Vent, K. M. Neyman, G. Pacchioni, and N. Rösch, *Chem. Phys. Lett.* **275**, 245 (1997).
- ⁷⁹V. Musolino, A. Selloni, and R. Car, *J. Chem. Phys.* **108**, 5044 (1998).
- ⁸⁰K. M. Neyman, V. A. Nasluzov, J. Hahn, C. R. Landis, and N. Rösch, *Organometallics* **16**, 995 (1997).
- ⁸¹G. Renaud, *Surf. Sci. Rep.* **32**, 1 (1998).
- ⁸²G. Haas, A. Menck, H. Brune, J. V. Barth, J. A. Venables, and K. Kern, *Phys. Rev. B* **61**, 11105 (2000).
- ⁸³Y. F. Zhukovskii, E. A. Kotomin, P. W. M. Jacobs, A. M. Stoneham, and J. H. Harding, *Surf. Sci.* **441**, 373 (1999).
- ⁸⁴V. V. Rivanenkov, V. A. Nasluzov, A. B. Gordienko, K. M. Neyman, U. Birkenheuer, and N. Rösch (unpublished).